

## Impedance analysis of oil conductivity and pixel non-uniformity in electrowetting displays

Bojian Xu<sup>a,b,1</sup>, Yuanyuan Guo<sup>a,b,1</sup>, Jitesh Barman<sup>b,c</sup>, Ben H. Ern e<sup>e</sup>, Yong Deng<sup>a,b</sup>, Guofu Zhou<sup>a,b,d,f</sup>, Jan Groenewold<sup>b,e</sup>

<sup>a</sup> Shenzhen Guohua Optoelectronics Tech. Co. Ltd, Shenzhen 518110, People's Republic of China

<sup>b</sup> Guangdong Provincial Key Laboratory of Optical Information Materials and Technology & Institute of Electronic Paper Displays, South China Academy of Advanced Optoelectronics, South China Normal University, Guangzhou 510006, People's Republic of China

<sup>c</sup> Department of Physics, Coochbehar College, Coochbehar Panchanan Barma University, Coochbehar, West Bengal 736101, India

<sup>d</sup> National Center for International Research on Green Optoelectronics, South China Normal University, Guangzhou 510006, People's Republic of China

<sup>e</sup> Van 't Hoff Laboratory for Physical and Colloid Chemistry, Debye Institute for Nanomaterials Science, Utrecht University, Padualaan 8, 3584 CH Utrecht, Netherlands

<sup>f</sup> Academy of Shenzhen Guohua Optoelectronics, Shenzhen 518110, People's Republic of China

### ARTICLE INFO

#### Keywords:

Electrowetting display devices  
Electrical impedance spectroscopy  
Equivalent-circuit analysis

### ABSTRACT

The electrical conductivity of the oil film is a key property of electrowetting displays (EWD) and its evolution probably correlates to the device lifetime. In this report, we fabricate an EWD device and measure its electrical impedance spectrum. The experimental results inform on the electrical resistivity of the oil film, as revealed by comparison with numerical simulations based on an equivalent electrical circuit model. Wide distribution in the oil-film resistance has to be incorporated into the model to reproduce the measured impedance spectrum precisely, which supports previous work indicative of pixel-to-pixel variation in the oil film electrical conductivity. Our work demonstrates that one can conveniently characterize the oil film resistance and its non-uniformity using electrical impedance spectroscopy.

### Introduction

Electrowetting displays (EWD) have the prospect of replacing electrophoretic displays (EPD) as the next generation of reflective color displays because EWDs can perform at video-speed [1–3]. Since they were invented [1], EWDs have been attracting extensive interest in both academia and industry. In academia, a focus of research has been on the physics and chemistry of the electrowetting phenomenon [2,4–9]. From an electro-mechanical perspective, electrowetting on dielectric (EWOD) involves an electrostatic force, usually called “electrowetting force ( $F_{EW}$ )”, exerted on the charge accumulated at the oil-substrate-conducting liquid triple contact line (TCL) due to the external electric field, thereby enabling the movement of the TCL and modifying the wetting behavior of the droplet on the dielectric substrate [8].

The basic structure of an EWD device usually consists of a bottom ITO/glass plate covered with a layer of dielectric and hydrophobic material which is often fluoropolymer (FP), as schematically shown in Fig. 1(a). A layer of photoresist (PR) material is patterned on top of the dielectric layer to form pixels where colored oil is present. The oil is a solution in which color dye is dissolved in nonpolar organic solvent.

Above the oil is the conductive liquid, which is water in this report. The device is covered with a top ITO/glass plate in contact with the conductive liquid and sealed by a peripheral frame (not shown in the figure). When no sufficient voltage is applied across the device, the ambient light incident on and reflecting from the device passes through the oil film, and hence it is partially absorbed by the oil, thereby rendering the color of the oil, which is called the “Off” state, as shown in Fig. 1(a). Upon applying a sufficient voltage across the device, the oil film ruptures due to the electric field across the oil film, allowing the water to contact, spread on FP and subsequently push the oil to the corner of the pixel because of the electrowetting force, thereby rendering the color of the substrate, which is called the “ON” state, as shown in Fig. 1(b).

Unfortunately, an oil backflow phenomenon occurs [11]. When the device is On and the voltage is kept constant, the open ratio (defined as the ratio of the water-covered area and the total area) continues to decrease in time. This phenomenon severely damages the display quality and hampers the commercialization of the EWD technique.

The oil backflow is usually ascribed to the charge trapping in or even leakage through FP [3,8,11–13]. Superposing a periodic transient

E-mail addresses: [xbj19870314@gmail.com](mailto:xbj19870314@gmail.com) (B. Xu), [jiteshb.iitk@gmail.com](mailto:jiteshb.iitk@gmail.com) (J. Barman), [jg@denk-werk.nl](mailto:jg@denk-werk.nl) (J. Groenewold).

<sup>1</sup> Bojian Xu and Yuanyuan Guo contributed equally to this work.

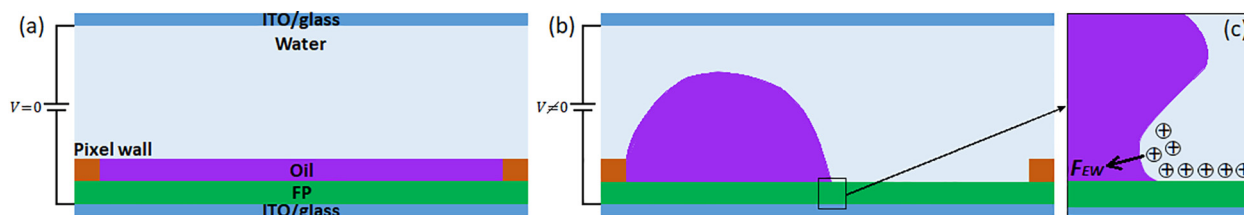


**Fig. 1. Schematic of the structure and working principle of the EWD device.** (a): When no voltage is applied across the device, the oil-film does not rupture. (b) When sufficient voltage is applied across the device, the oil-film ruptures and is pushed to the corner of the pixel while the water is spreading on FP. (c) The charge accumulates around the TCL and the electrowetting force is generated, pulling the TCL and pushing the oil leftwards, leading to the spreading of the water on FP. The device is adapted from Ref. [10], and the rightmost zoom-in drawing is inspired by Ref. [6].

reset signal on the driving voltage is usually employed to maintain the apparent display status [14–17]. However, this type of driving scheme also increases power consumption significantly [18], thereby decreasing the competitive advantage of the EWD technique, compared to other display techniques. Adding more insulating dielectric layers below FP can also suppress the undesired effect.

Besides the charge trapping and leakage, there can be other mechanisms causing a decrease in charge density. The oil is usually assumed to be insulating [19]. However, it can have finite electrical conductivity due to the following reasons, thereby leading to charge leakage through the oil and the oil backflow. Ions in the water can also protonate the dye molecules in the oil, therefore being transferred into the oil in the presence of an electric field [9,20,21]. Besides, inverse micelles can also generate when non-polar dyes are ionized and then aggregate in the oil [9,22,23]. These possible mechanisms responsible for oil conductivity have not been fully investigated, but it is clear that the oil backflow is related to the dye concentration and its chemical structure [11,24].

Another undesired phenomenon is the non-uniform rupture of the oil film, which has been reported and attributed to inhomogeneous oil conductivity [10]. We found that our newly-prepared oil has a conductivity on the order of  $\sim 10^{-12}$ – $10^{-11}$  S/m. However, the oil experiences degradation processes which lead to a non-uniform increase in oil conductivity after being filled into the pixels.

The above-undesired phenomena have drawn our attention to the investigation of the electrical conductivity of the oil, its effect on the display quality of the EWD device and evolution during the device lifetime. Therefore, we set out to characterize the electrical conductivity of the oil without disassembling the device. Evaluation of the electrical conductivity of the oil through measuring the current–voltage relation of the whole device requires assumptions regarding the electrical properties of the FP. Moreover, this method cannot be used to investigate the uniformity in the oil of the pixels. To obtain more information, we turned to electrical impedance spectroscopy. The frequency dependence of the impedance and the dissipation factor of the EWD device is measured and simulated based on an equivalent electrical circuit model. Through this research, we show the effect of oil conductivity and its non-uniformity on frequency dependence. The result in this report demonstrates that the impedance analysis is a feasible and convenient method to characterize the oil conductivity. The effect that is shown in this report also reinforces the former assumption about distribution in the oil film conductivity.

## Experimental

### EWD device fabrication

The bottom substrate was an ITO/glass with the sheet resistance of  $100 \Omega/\square$ . It was adequately cleaned in detergent and then dried at  $120^\circ\text{C}$  in an oven for 2 h. 4.2 wt% amorphous fluoropolymer (FP) (AF1600, Chemours, with the dielectric constant of 1.934) solution was spin-coated on the substrate at 1500 rpm, and then cured at  $185^\circ\text{C}$  in

an oven for 1 h. The substrate was then activated by reactive ion etching (RIE) to change the surface from hydrophobic state to hydrophilic state, to spin coat a negative photoresist (PR). The thicknesses of FP and PR were always monitored using a profilometer (Bruker DektakXT). The pixels were formed after the photolithography process. After the device was heated above the glass transition temperature,  $T_g$ , of FP ( $160^\circ\text{C}$ ) in the oven for 2 h, the hydrophobic state of FP was recovered. Then, the colored oils were filled into the pixels uniformly using a raster filling method underwater at the speed of  $\sim 1$  mm/s. In the end, the device was covered with a top ITO/glass and sealed by the acrylic glue.

### Oil formulation

The anthraquinone purple dye (purity  $\geq 98\%$ ) was purchased from a local company (Jiaxing Evershine Chemical co. LTD.). The oil was formulated by dissolving the dye in decane (Aldrich,  $\geq 99\%$ , with a dielectric constant of 2.2) with a concentration of 10 wt%. This oil is called the low-conductivity-oil in this report. To study the effect of oil conductivity, we intentionally increase the oil conductivity; the non-polar decahydronaphthalene (Macklin,  $\geq 97\%$ ) was mixed with decane with volume ratio 1:1, and then the dye was dissolved into the mixed solvent to formulate the oil. The dye concentration was kept constant. To further increase the oil conductivity, lauric acid (Aldrich,  $\geq 98\%$ ), a surfactant, was also added with a concentration of 2.5 wt%, in addition to decahydronaphthalene. The latter two types of modified oil are called the high-conductivity oil in this report.

### Oil conductivity measurement

The oil conductivity was measured right after the formulation using Guangzhou Zihui DPCM-11/YX1154 (accuracy 0.01 pS/m). 100 mL of formulated oil was filled into the testing cell. The conductivity of the oil was measured with 5 V DC within 3 sec. The value was the average of two readings with different electrode polarities. The measurement proceeded in a cleanroom at the temperature of  $25 \pm 2^\circ\text{C}$  and the relative humidity of 50%.

### Impedance spectroscopy measurement

A “PMC 1000 Potentiostat” (Princeton Applied Research) was used to measure the device with the low-conductivity oil, and the “CHI660E” electrochemical workstation (CH Instruments, Inc.) was used to measure the devices with the high-conductivity oil. Control experiments were performed by using the second equipment to measure the device with the low-conductivity oil; similar results were achieved. The top ITO plate was connected to the working electrode (WE) and the sense electrode (SE), and the bottom ITO substrate was connected to the counter electrode (CE) and the reference electrode (RE). An AC voltage of 0.5 Vrms was applied to the top ITO plate. The frequency of the voltage was varied from  $10^4$  Hz to  $10^{-2}$  Hz, 10 (12 for the second equipment) steps per decade. DC bias was set to zero.

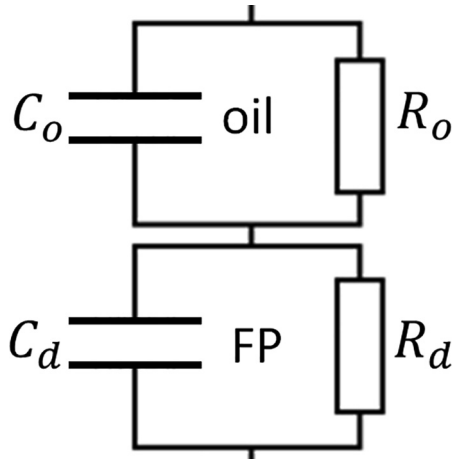


**Fig. 2.** Equivalent electrical circuit of a pixel of an EWD device.  $R_o$ ,  $C_o$ ,  $R_d$  and  $C_d$  are the resistance and capacitance of the oil film and the resistance and capacitance of FP, respectively.

### Equivalent circuit model

**Fig. 2** shows the equivalent circuit of a pixel. An aqueous phase is in series with the drawn impedance elements, but considering its much larger conductivity and dielectric constant compared to the oil and FP, and also considering the maximum frequency of  $10^4$  Hz in our measurements, the impedance of the aqueous phase is neglected in this report. The four circuit parameters,  $R_o$ ,  $C_o$ ,  $R_d$  and  $C_d$  are the resistance and capacitance of the oil film and the resistance and capacitance of FP, respectively. When a DC voltage is applied to the device, the current flows only through  $R_o$  and  $R_d$ . In this case, the dissipation is caused by the current flow through the two resistances. When an AC voltage is applied to the device, the current flows through both the capacitors and the resistors, leading to the dissipation factor  $D = \omega RC$ , which increases with frequency  $\omega$ . The competition between the two paths depends on the magnitude of the impedances ( $Z$ ) of the paths. At very high frequencies, the impedance due to the capacitors become so small that the current flowing through the two resistances can be neglected, leading the current flow mainly through the two capacitors and zero dissipation. Hence, as the frequency of the applied voltage varies from low to high,  $D$  firstly drops quickly, then increases to a local maximum dissipation factor ( $D_{peak}$ ) at a certain frequency ( $f_{peak}$  or  $\omega_{peak} = 2\pi f_{peak}$ ), and then approaches to zero, as shown in **Fig. 3b**. Expressions for the impedance and the dissipation factor are given in Eqs. (1) and (2). They describe the frequency spectrum, including the width of the peak in  $D(\omega)$ , in the case of a uniform system where the oil has the same conductivity  $R_o$  in each pixel:

$$Z(\omega) = \frac{R_o}{1 + \omega^2 C_o^2 R_o^2} + \frac{R_d}{1 + \omega^2 C_d^2 R_d^2} - j \left( \frac{\omega C_o R_o^2}{1 + \omega^2 C_o^2 R_o^2} + \frac{\omega C_d R_d^2}{1 + \omega^2 C_d^2 R_d^2} \right) \equiv Z'(\omega) - jZ''(\omega) \quad (1)$$

$$D(\omega) = \frac{Z'(\omega)}{Z''(\omega)} = \frac{B}{\omega + \frac{A}{\omega}} + \frac{C}{\omega^3 + E\omega} \quad (2)$$

Eq. (1) is the analytical expression for the angular-frequency dependence of the circuit impedance  $Z(\omega)$  which consists of  $Z'$  and  $Z''$  as the real and imaginary parts, respectively. The angular-frequency dependence of the dissipation factor  $D(\omega)$  is the ratio of  $Z'$  to  $Z''$  and can be written into the form of Eq. (2), where  $A$ ,  $B$ ,  $C$  and  $E$  are the functions of the four circuit parameters. In this way, we can see that the second term  $D(\omega)$  monotonically decreases with  $\omega$ , while the first term has a local maximum at  $\omega_{peak} = \sqrt{A}$ , indicating that  $D(\omega)$  has a local maximum. To plot the frequency dependence of  $Z'(f)$ ,  $Z''(f)$  and  $D(f)$  based

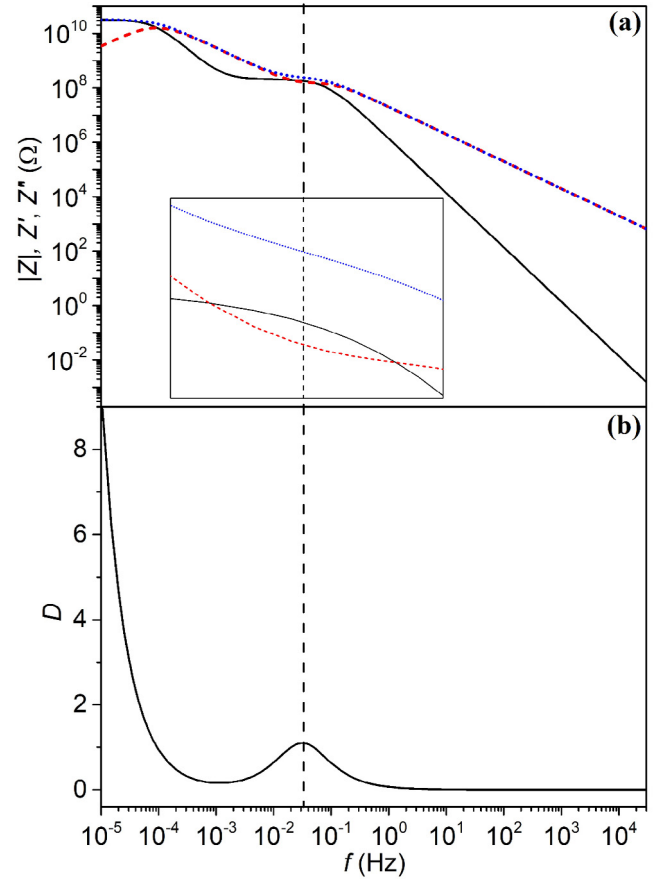


**Fig. 3.** Plot of Eq. (1) and (2) as a function of frequency. (a): Frequency-dependence of  $Z'$  (black solid),  $Z''$  (red dash) and  $|Z|$  (blue dot). The inset zooms in on the part of the plot between  $10^{-2}$  Hz and  $10^{-1}$  Hz. (b): Frequency-dependence of  $D$ . The vertical dashed line at  $\sim 0.03$  Hz in (a) and (b) indicates the position of the peak. (For interpretation of the references to color in this figure legend, the reader is referred to the web version of this article.)

on Eq. (1) and (2), the circuit parameters are calculated according to Ref. [10]. The area of the pixel is set to  $185 \times 185 \mu\text{m}^2$ . The oil-film thickness  $t_o$  and the FP thickness  $t_d$  are set to  $5.5 \mu\text{m}$  and  $850 \text{ nm}$ , respectively. The oil conductivity  $\sigma_o$  and the FP conductivity  $\sigma_d$  are set to  $1 \times 10^{-11} \text{ S/m}$  and  $1 \times 10^{-14} \text{ S/m}$ , respectively. The dielectric constant of the oil  $\epsilon_{ro}$  and that of FP  $\epsilon_{rd}$  are set to 2.2 and 1.934, respectively. **Fig. 3(a)** shows that  $Z'$  decreases with the frequency.  $Z''$  first increases then decrease with the frequency. There is a transitional regime between  $10^{-2}$  Hz and  $10^{-1}$  Hz, where the rate of the decrease is moderated and  $Z'$  becomes larger than  $Z''$  in the frequency regime of about 0.02 Hz to 0.05 Hz. **Fig. 3(b)** reveals the local maximum dissipation factor at  $\sim 0.03$  Hz, correlated to the transition regime. The calculation result suggests that the peak  $D$  occurs when the real part of the impedance reaches the same order of magnitude as the imaginary part, which implies that the resistive dissipation becomes more dominant when the peak frequency is approached.

The peak frequency,  $\omega_{peak}$ , can be expressed as a function of the time constant of the oil film  $\tau_o = \epsilon_0 \epsilon_{ro} / \sigma_o$  ( $\epsilon_0$  is the vacuum permittivity),  $C_o/C_d$  and  $R_o/R_d$ . Since  $\tau_o$ ,  $C_o/C_d$  and  $R_o/R_d$  are correlated,  $\omega_{peak}$  is expressed using Eq. (3), assuming that  $t_o/t_d$ ,  $\epsilon_{ro}$ ,  $\epsilon_{rd}$ ,  $\sigma_d$  and  $\sigma_o$  are independent of each other:

$$\omega_{peak} \left( \frac{t_o}{t_d}, \epsilon_{ro}, \epsilon_{rd}, \sigma_d, \sigma_o \right) = \frac{1}{\epsilon_0} \sqrt{\frac{1}{\epsilon_{ro} \epsilon_{rd}}} \sqrt{\frac{1}{\frac{t_o}{t_d} + \frac{\epsilon_{ro}}{\epsilon_{rd}}}} \sqrt{\sigma_o^2 + \sigma_d^2 \frac{t_o \epsilon_{ro}}{t_d \epsilon_{rd}}} \quad (3)$$

It is worth mentioning that, based on Eq. (3), if  $\sigma_d \ll \sigma_o$  and  $\epsilon_{ro} t_o / (\epsilon_{rd} t_d) \sim 1$ ,  $\omega_{peak}$  is approximately proportional to  $\sigma_o$ . By fixing

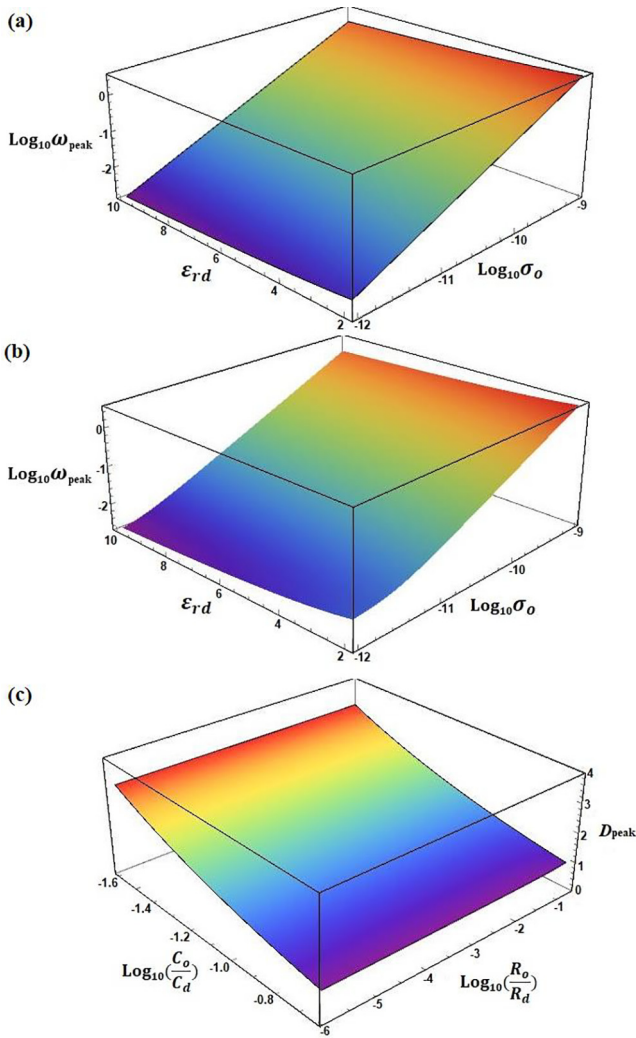


**Fig. 4.** Effect of the oil conductivity and the dielectric constant of FP on the peak position, and effect of the ratio of the oil and FP capacitances, and the ratio of the oil and FP resistances on the peak height. (a) and (b): Plot of  $\omega_{peak}$  as a function of  $\epsilon_{rd}$  and  $\sigma_o$  according to Eq. (3), with  $\sigma_d$  of  $10^{-14}$  S/m and  $10^{-12}$  S/m, respectively. (c): Plot of  $D_{peak}$  as a function of  $C_o/C_d$  and  $R_o/R_d$  according to Eq. (4).

$t_o/t_d$  at  $5.5 \mu\text{m}/850 \text{ nm}$  and setting  $\sigma_d$  to  $10^{-14}$  S/m and  $10^{-12}$  S/m,  $\omega_{peak}$  is plotted as a function of  $\epsilon_{rd}$  and  $\sigma_o$ , as shown in Fig. 4(a) and (b), respectively. We can see that both increasing in  $\sigma_o$  and decreasing in  $\epsilon_{rd}$  lead to an increase in  $\omega_{peak}$ . However,  $\sigma_o$  causes a much stronger effect in  $\omega_{peak}$  than  $\epsilon_{rd}$  does. There is no significant difference between the calculations for two different  $\sigma_d$ . Plots at different  $t_o/t_d$ , which are omitted here, also show no distinct difference.

Setting  $\omega = \omega_{peak}$  in Eq. (2), one gets  $D_{peak}$ , which can be expressed as a function of the relative value of the two capacitances  $C_o/C_d = \epsilon_{ro} t_d / (\epsilon_{rd} t_o)$ , and the relative value of the two resistances  $R_o/R_d = \sigma_d t_o / (\sigma_o t_d)$ , as shown in Eq. (4):

$$D_{peak} \left( \frac{C_o}{C_d}, \frac{R_o}{R_d} \right) = \frac{1}{2} \sqrt{\frac{\frac{C_o}{C_d} + 1}{\left( \frac{C_o}{C_d} \right)^2 \left( \frac{R_o}{R_d} \right)^2 + \frac{C_o}{C_d}} \left[ \frac{\left( \frac{C_o}{C_d} \right)^2 \frac{R_o}{R_d} + 1}{\frac{C_o}{C_d} + 1} + \frac{\frac{C_o}{C_d} \left( \frac{R_o}{R_d} \right)^2 + \frac{C_o}{C_d} \frac{R_o}{R_d}}{\frac{C_o}{C_d} \left( \frac{R_o}{R_d} \right)^2 + 1} \right] \quad (4)$$

To plot  $D_{peak}$ ,  $C_o/C_d$  and  $R_o/R_d$  need to be set in a certain range.  $t_o$  and  $t_d$  are considered to be in the range of  $5.5 \pm 0.5 \mu\text{m}$  and  $850 \pm 150 \text{ nm}$ ,

respectively.  $\sigma_o$  of the newly-prepared purple oil was found to be on the order of magnitude of  $10^{-12}$  S/m to  $10^{-11}$  S/m. It was also found that  $\sigma_o$  increases when water blends into the oil or charge transfers from water into the oil [9,10]. Hence,  $\sigma_o$  is set in the range of  $[10^{-12}, 10^{-9}]$  S/m. Due to its nanoporosity, FP is electrically leaky when directly contacting with the water.  $\sigma_d$  is therefore set in the range of  $[10^{-14}, 10^{-12}]$  S/m. The penetration of water molecules into the porous FP can also cause an increase in  $\epsilon_{rd}$  [25–27]. Besides the penetration, the hydroxide ions also tend to adsorb to FP [28], which can introduce dipoles in FP, thereby increasing effective  $\epsilon_{rd}$  of FP. Hence, a range of  $[1.934, 10]$  is given to  $\epsilon_{rd}$ . Based on the above settings,  $C_o/C_d$  is in the range of  $[0.025, 0.23]$  and  $[1.17 \times 10^{-6}, 0.2]$  for  $R_o/R_d$ . As shown in Fig. 4(c),  $D_{peak}$  does not vary noticeably with the varying of  $R_o/R_d$ , while it increases sensitively when  $C_o/C_d$  decreases, which indicates that the local maximum dissipation factor sensitively depends on  $\epsilon_{rd}$  and  $t_d/t_o$  if we consider that the variation in  $\epsilon_{ro}$  is assumed to be very limited for the low-conductivity-oil.

The non-uniform decay time of the pixels has been ascribed to the nonuniform oil conductivity of the pixels of the EWD device [10]. Hence, the distribution of  $R_o$  should be taken into account when modeling the frequency dependences of  $|Z|$  and  $D$ . The mechanism of the evolution of the oil conductivity is not fully understood and the precise distribution of  $R_o$  is not known. Distribution types in the exponential family, for example, the Exponential, Gamma, Log-Normal, Inverse-Gaussian, Inverse-Gamma distributions, are often adopted to build statistical models for skewed data sets and to analyze and forecast failure and degradation. One can see from Fig. S1 in the Supplementary material [29] that all the Exponential, Gamma, Log-Normal distributions can describe the measured spreading of  $R_o$ . To discriminate between different types of distributions and to choose the most suitable one can in principle be done based on the statistical properties of the mechanisms that cause change in  $R_o$ . This report will not explore this subject in detail. For convenience, we will assume a Gamma distribution in most of our calculations and compare the outcome with calculations that assume two other types of distribution. To incorporate the distribution into the model, numerical integration is used to calculate the total impedance and the dissipation factor, which is described schematically in Fig. S2 in the Supplementary material [29]. The device modeling also needs to take account of the “rest” region of the device, including the region where the water directly contacts PR, the region of the sealing frame, and the air gap between the top and bottom ITO plates, as shown in Fig. S3 in the supplementary material [29].

## Results and discussion

The measured frequency-dependences of  $|Z|$  and  $D$  of the low-conductivity-oil device are modeled using the above equivalent-circuit model with a Gamma distribution of  $R_o$ . The probability density function (PDF) of the distribution, plotted with the cyan line in Fig. 6(a), has the shape parameter  $\alpha = 1.25$  and hence the scale parameter  $\beta = 1.5 \times 10^{13} \Omega$ . The measured results can be modeled very well by taking the value of the modeling parameters listed in Table 1, as shown in Fig. 5. The oil conductivity is set to  $7 \times 10^{-12}$  S/m, leading to an average  $R_o$  of  $\sim 1.8 \times 10^{13} \Omega$  which lies in the high-resistance regime of Fig. S1 [29]. It is found that only the newly-prepared low-conductivity oil has the conductivity on the order of  $10^{-12}$  S/m. When water is mixed with the oil, the conductivity rises, varying between  $10^{-12}$  S/m and  $10^{-9}$  S/m. The derived  $\sigma_o$  therefore implies that there is no significant mixing of water in the oil.

### Effect of the shape parameter on the device modeling

Fig. 5 also shows the modeled results of setting  $\alpha$  to 5 and 0.71, and the result without using any distribution. The PDFs of the Gamma distributions with different  $\alpha$ , and the evolving trend of the peak as  $\alpha$  changes are plotted in Fig. 6. In addition to the peak values of the

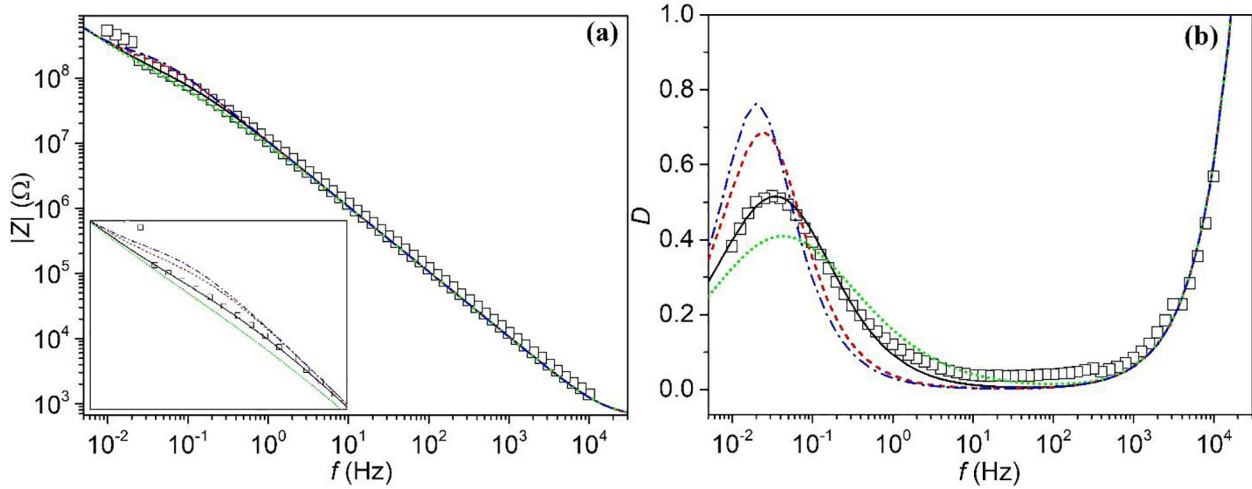


**Fig. 5. Experimental (symbols) and modeled (lines) results of the frequency-dependence of  $|Z|$  (a) and  $D$  (b).** The measured EWD device is filled with low-conductivity oil. The blue dash-dot lines are the plot of the modeled result without the incorporation of any distribution of  $R_o$ . The other three lines are the plots of the modeled results with incorporation of a Gamma distribution of  $R_o$ , which has the scale parameter ( $\beta$ ) and the shape parameter ( $\alpha$ ) of  $1.5 \times 10^{13} \Omega$  and 1.25 (black solid, good fit of peak),  $3.7 \times 10^{12} \Omega$  and 5 (red dash, overestimated peak),  $2.6 \times 10^{13} \Omega$  and 0.71 (green dot, underestimated peak). The values of the other modeling parameters are listed in Table 1. (For interpretation of the references to color in this figure legend, the reader is referred to the web version of this article.)

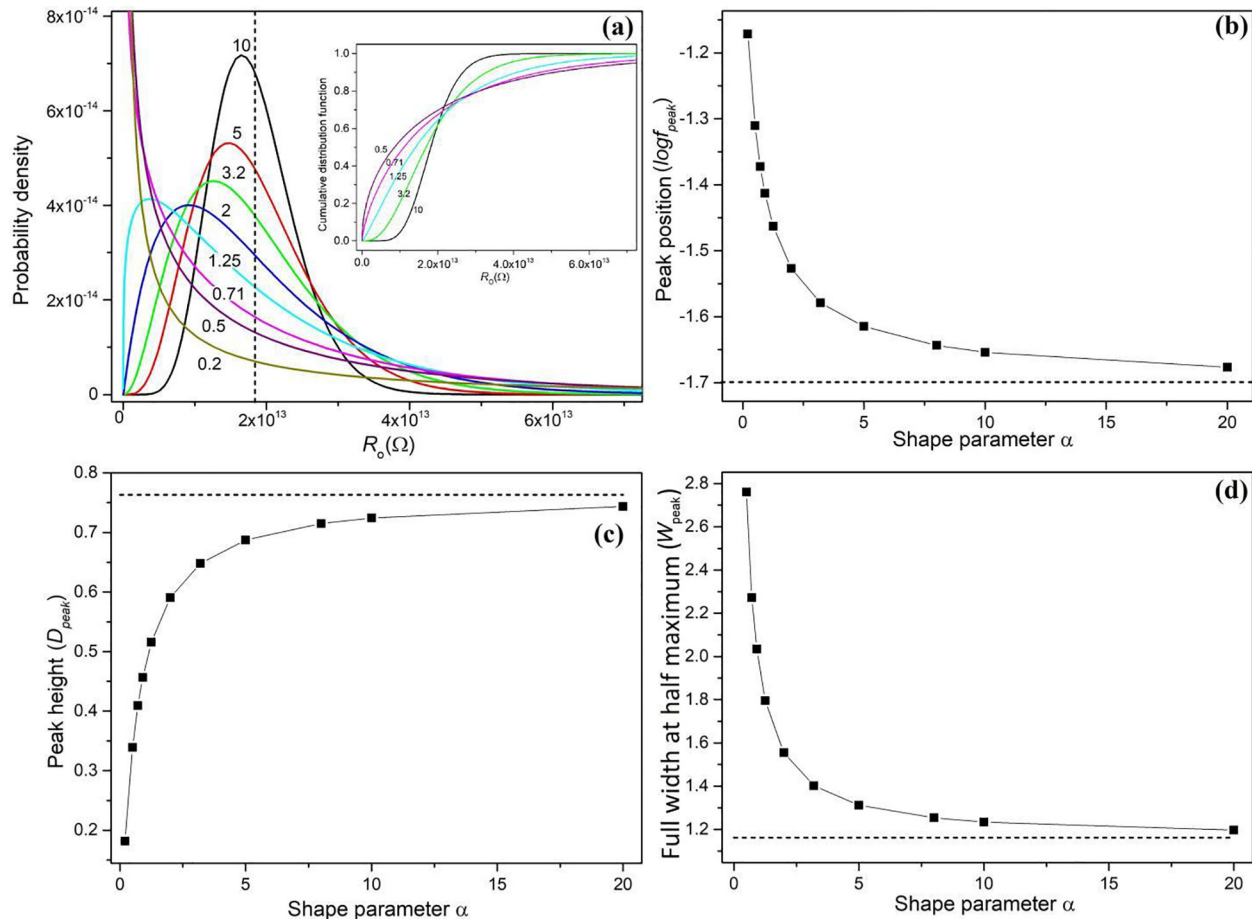


**Fig. 6. Effect of the shape parameter of the Gamma distribution PDF on the shape of the peak of the dissipation factor.** (a): The Gamma distribution PDFs with different shape parameters denoted by the numbers in the subfigure. The cumulative distribution functions (CDFs) of several shape parameters are shown in the inset. The average  $R_o$  is fixed and denoted by the dashed line. (b): Effect of the shape parameter on the peak position. (c): Effect of the shape parameter on the peak height. (d): Effect of the shape parameter on the half-peak width. The dashed lines in (b)-(d) denote the results modeled without the incorporation of any distribution.

**Table 1**

The value of the parameters corresponding to the modeled result (black solid line) in Fig. 5.

Parameter	Value	Unit
$\sigma_o$	$7 \times 10^{-12}$	S/m
$\sigma_d$	$1 \times 10^{-14}$	S/m
$\epsilon_{ro}$	2.2	–
$\epsilon_{rd}$	1.934	–
$t_o$	4.5	$\mu\text{m}$
$t_d$	817	nm
$\beta$	$1.5 \times 10^{13}$	$\Omega$
$R_{ESR}$	650	$\Omega$

frequency and the dissipation factor,  $f_{peak}$  and  $D_{peak}$ , the peak width  $W_{peak}$  is also used to describe the peak ( $W_{peak}$  is here the full width at half maximum, that is, the difference of the logarithmic value of the frequencies that lead to  $D = D_{peak}/2$  on both sides of the peak). It can be seen from Figs. 5 and 6 that the modeled result without using any distribution, which can be regarded as the narrowest distribution, has the smallest  $W_{peak}$ , the largest  $D_{peak}$ , and the smallest  $f_{peak}$ . As  $\alpha$  decreases, the PDF becomes more and more broadened, and the peak becomes more and more lowered and broadened, and shifts to the higher frequency regime.

### Effect of the oil conductivity on the device modeling

The influence of  $\sigma_o$  on the modeled results is examined by comparing the effects of the oil conductivity being  $7 \times 10^{-11}$  S/m or  $7 \times 10^{-10}$  S/m, see Fig. 7. The modeled result reveals that the peak position  $f_{peak}$  shifts to the higher-frequency regime as  $\sigma_o$  increases. There is no distinct change in the shape of the peak. The effect of the oil conductivity on the impedance modelling results reveals how the shape parameter directly affects the dissipation peak. As the shape parameter  $\alpha$  decreases while the mean oil film resistance  $R_o$  is fixed, the Gamma distribution PDF becomes more and more broad and right-skewed (as shown in Fig. 6a). This means that the number of pixels with smaller oil-film resistance increases (as shown in the inset of Fig. 6a). These pixels have different maximum dissipation locating at different and higher frequencies. Hence, broader dissipation peaks with smaller  $D_{peak}$  and larger  $f_{peak}$  are obtained when incorporating a Gamma distribution with a more right-skewed PDF in the calculation of the frequency dependence of impedance, as shown in Fig. 5b. Fig. 8 exhibits the

measurement and modeled results of the two high-conductivity-oil devices. The measured  $\sigma_o$  is  $1 \times 10^{-9}$  S/m for the oil with only decahydronaphthalene added, and  $7 \times 10^{-9}$  S/m for the one with both decahydronaphthalene and the surfactant added. The measured frequency dependence  $D$  of the two devices shows that the peak position shifts by a factor of 10, which verifies the modeled trend that  $f_{peak}$  increases with  $\sigma_o$ . However,  $\sigma_o$  is set to  $2 \times 10^{-9}$  S/m in the modeling for the oil of lower conductivity, while it is set to  $0.8 \times 10^{-9}$  S/m for the oil of higher conductivity, which is in contradiction with the trend. This mismatch is probably because of a surfactant in the water, thereby causing the real  $\sigma_o$  of the oil containing the surfactant to be lower than the value measured right after the preparation of the oil.

### Effect of the other parameters on the device modeling

The effects of the other parameters,  $\epsilon_{ro}$ ,  $\epsilon_{rd}$ ,  $t_o$ ,  $t_d$ ,  $R_{ESR}$  and  $\sigma_d$ , on the modeling results are also examined. The results are plotted in Figs. S4–S10 in the Supplementary material [29]. The broadness of the measured peak cannot be explained by varying those parameters in the device modeling. It is found that increases in  $\epsilon_{ro}$  also decreases  $D_{peak}$  and renders the peak more broadened, as shown in Fig. S4. However,  $|Z|$  decreases distinctly as well, which cannot be compensated efficiently by varying other parameters. Moreover, it is not realistic that  $\epsilon_{ro}$  increases to 6 for the low-conductivity-oil. Hence, the decreasing in  $D_{peak}$  and broadening of the peak cannot be explained by an increasing in  $\epsilon_{ro}$ . In contrast, increasing in  $\epsilon_{rd}$  causes remarkable increase in  $D_{peak}$ , which matches the above discussion regarding Fig. 4(c), and it causes decrease in  $|Z|$  in the transition regime as well, as shown in Fig. S5. There is no noticeable change in the frequency regime to the right side of the peak. The opposite effects of  $\epsilon_{ro}$  and  $\epsilon_{rd}$  on the peak, and the effect of  $\sigma_o$  on the peak position, suggest that the peak is related to the current flowing through the resistance of the oil film and the charging of the capacitance of FP. It is worth mentioning that the increase in  $\epsilon_{ro}$  also increases  $D$  noticeably in the high-frequency regime above  $\sim 10^3$  Hz, as shown in Fig. S4(b). This dependence is much weaker while varying  $\epsilon_{rd}$ , as shown in Fig. S5(b). This is probably because when the frequency is high enough, the equivalent circuit shown in Fig. 3 can be regarded as  $C_o$  connected with  $C_d$  in series. So the total capacitance of the EWD device ( $C_{device}$ ) is mainly determined by  $C_o$  because  $C_o$  is smaller than  $C_d$ .

The oil-filling process can be incomplete, thereby rendering the oil-film thickness ( $t_o$ ) smaller than the height of the pixel wall, that is, the thickness of PR, which is  $5.5 \mu\text{m}$ .  $t_o$  is therefore set to  $5.5 \mu\text{m}$  and

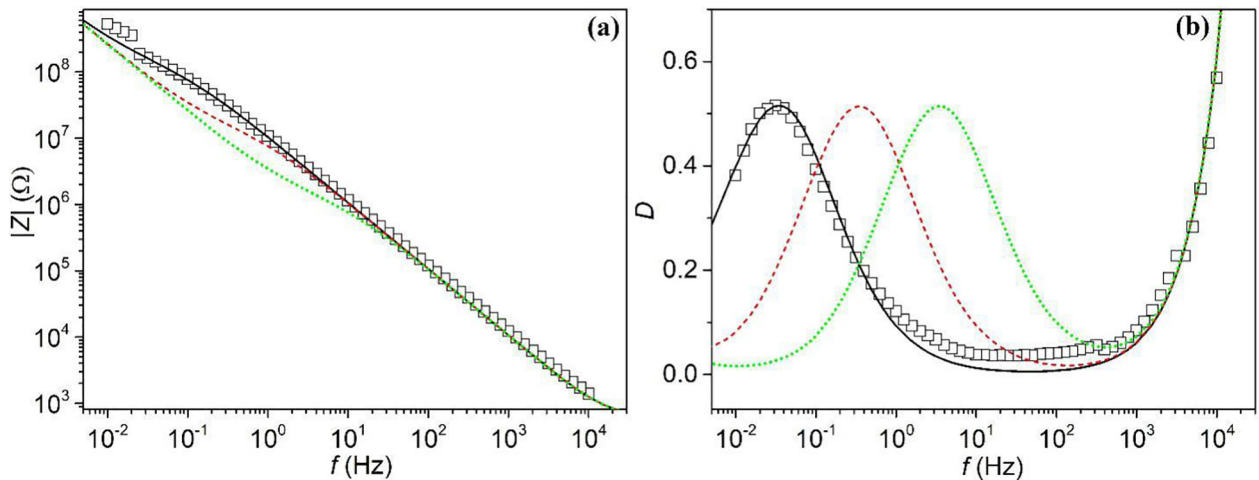


**Fig. 7.** Experimental (symbols) and modeled (lines) results of the frequency dependences of  $|Z|$  (a) and  $D$  (b). The measuring device is filled with the original purple oil. The Gamma distribution with the shape parameter of 1.25 is used in the modeling. The oil conductivity is set to  $7 \times 10^{-12}$  S/m (black solid, good fit),  $7 \times 10^{-11}$  S/m (red dash, underestimated  $|Z|$  and peak shifted by a factor of 10) and  $7 \times 10^{-10}$  S/m (green dot, more underestimated  $|Z|$  and peak shifted by a factor of 100). The value of  $\sigma_d$ ,  $\epsilon_{ro}$ ,  $\epsilon_{rd}$ ,  $t_o$ ,  $t_d$  and  $R_{ESR}$  is the same as listed in Table 1. (For interpretation of the references to color in this figure legend, the reader is referred to the web version of this article.)

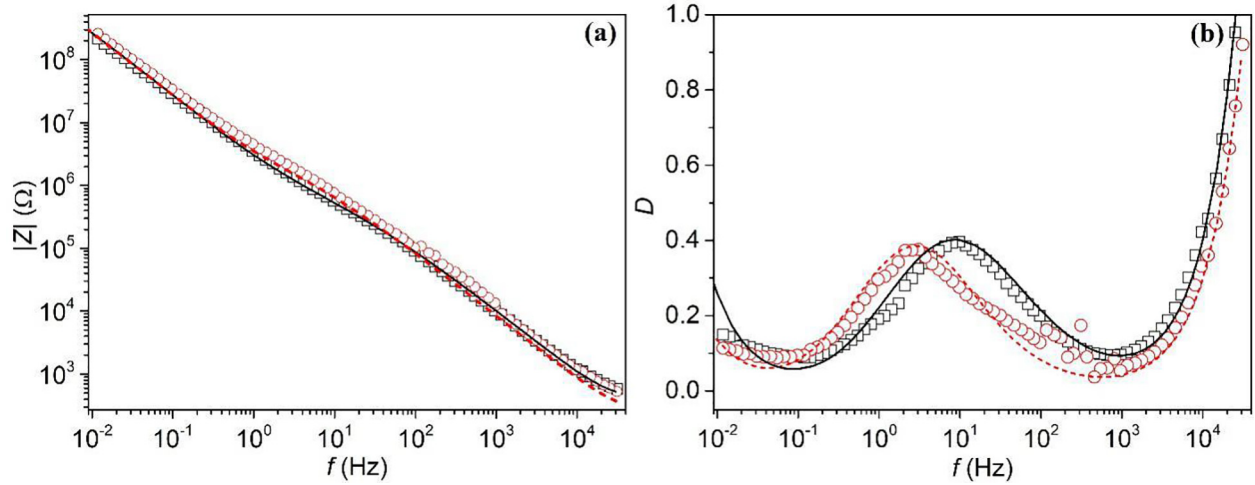


**Fig. 8. Experimental (symbols) and modeled (lines) results of the EWD devices.** The measuring devices are filled with the modulated oil which has the measured  $\sigma_o$  of  $1 \times 10^{-9}$  S/m (black squares) and  $7 \times 10^{-9}$  S/m (red circles). (a): Frequency-dependence of  $|Z|$ . (b): Frequency-dependence of  $D$ . The value of the parameters is listed in Table 2. A Gamma distribution is incorporated in the modeling. (For interpretation of the references to color in this figure legend, the reader is referred to the web version of this article.)

**Table 2**

The value of the parameters corresponding to the modeled results in Fig. 8.

Parameter	Value		Unit
	Black squares	Red circles	
$\sigma_o$	$2 \times 10^{-9}$	$0.8 \times 10^{-9}$	S/m
$\sigma_d$	$3 \times 10^{-13}$	$1.5 \times 10^{-13}$	S/m
$\epsilon_{ro}$	3.2	4.5	-
$\epsilon_{rd}$	1.934		-
$t_o$	5.6		$\mu\text{m}$
$t_d$	852	840	nm
$\beta$	$1.10 \times 10^{11}$	$2.54 \times 10^{11}$	$\Omega$
$R_{ESR}$	400	250	$\Omega$

3.58  $\mu\text{m}$  to examine the effect of the oil-film thickness on the simulation result. Fig. S6 shows that with increasing of  $t_o$ ,  $Z$  increases slightly over the whole calculated frequency regime. The increasing rate of  $Z$  varies between 3% and 13% over the frequency regime when the oil film thickness increases from 3.58  $\mu\text{m}$  to 4.5  $\mu\text{m}$  or from 4.5  $\mu\text{m}$  to 5.5  $\mu\text{m}$ , as shown in Fig. S6(c). In contrast, the increasing rate of  $D$  varies differently with the frequency when  $t_o$  rises. One can see in Fig. S6(d) that the increasing rate decreases with the frequency, being positive when the frequency is smaller than  $\sim 1$  Hz while negative in the larger frequency regime. Figs. S6(e) and (f) demonstrate that  $f_{\text{peak}}$  increases while  $D_{\text{peak}}$  decreases with the oil film thickness. Furthermore, we define  $D_{\text{peak}}/W_{\text{peak}}$  as the dissipation peak sharpness coefficient. It is shown in Fig. S6(g) that the peak sharpens with the oil film thickness. The effect of  $t_o$  on  $D_{\text{peak}}$  can be understood from Fig. 4(c) which shows that  $D_{\text{peak}}$  increases when  $C_o$  turns smaller. The effect of  $t_o$  on  $f_{\text{peak}}$  is in line with the effect of  $\sigma_o$  on the peak discussed above. An increase in  $t_o$  can be regarded as a decrease in  $\sigma_o$  in the equivalent circuit system, thereby causing the peak to shift to the lower frequency regime. The slight

**Table 3**

The value of the parameters corresponding to the modeled results in Fig. 9.

Parameter	Value			Unit
	Black solid (Gamma)	Red dash (Exponential)	Green dot (Log-Normal)	
$\sigma_o$	$7 \times 10^{-12}$	$6 \times 10^{-12}$	$4.5 \times 10^{-12}$	S/m
$t_o$	4.5	5.3	4.5	$\mu\text{m}$
Distribution parameters	Scale parameter $\beta = 1.50 \times 10^{13} \Omega$ Shape parameter $\alpha = 1.25$	Rate parameter $\lambda = 4.21 \times 10^{-14} \Omega^{-1}$	Standard deviation $\sigma = 1.10$ Mean parameter $\mu = 30.38$	-

variation in the peak shape (from 0.53 to 0.62) suggests that the difference in the broadness of the measured peak (peak sharpness coefficient 0.56) and the modeled peak without using any distribution (peak sharpness coefficient  $\sim 10$ , blue dash-dot line in Fig. 5b) cannot be obtained by tweaking the oil film thickness between 5.5  $\mu\text{m}$  and 3.58  $\mu\text{m}$ .

Thickness of the FP layer ( $t_d$ ) of the EWD device with the original purple-oil is measured to be  $798 \pm 19$  nm. Varying  $t_d$  in the measured range does not lead to a distinct change in the modeling results, as shown in Fig. S7. The measured total capacitance of the EWD device is on the order of  $10^{-8}$  F and the equivalent series resistance is on the order of  $10^2$  to  $10^3 \Omega$ . The contribution to  $D$  due to  $R_{ESR}$ ,  $\omega R_{ESR} C_{\text{device}}$ , is therefore in the range of  $6.28 \times 10^{-6} f$  to  $6.28 \times 10^{-5} f$ . Hence, it can be expected that when  $f$  is larger than  $10^3$  to  $10^4$  Hz, the amount of the dissipation caused by  $R_{ESR}$  becomes more and more critical, thereby causing the total dissipation factor to be more sensitive to  $R_{ESR}$  in the high-frequency region, which is verified and shown in Fig. S8. Although the valley of the dissipation factor in the low-frequency regime to the left side of the peak cannot be fully characterized because of the limitation of the measurement equipment, it can still be concluded that the real  $\sigma_d$  is probably smaller than  $1 \times 10^{-13}$  S/m. As demonstrated in Fig. S9, an increase in  $\sigma_d$  leads to a noticeable increase in  $|Z|$  and  $D$  in the low-frequency regime. When  $\sigma_d$  is set to  $1 \times 10^{-12}$  S/m, the rising tendency of  $D$  with frequency turns into a decreasing tendency. Introducing a Gamma distribution of  $R_d$  also lifts the valley, as exhibited in Fig. S10.

### Using different types of distributions for the device modeling

Besides using the Gamma distribution, the Exponential and Log-Normal distributions have also been tried. The values of the distribution parameters are listed in Table 3.  $\sigma_o$  and  $t_o$  are set differently for different

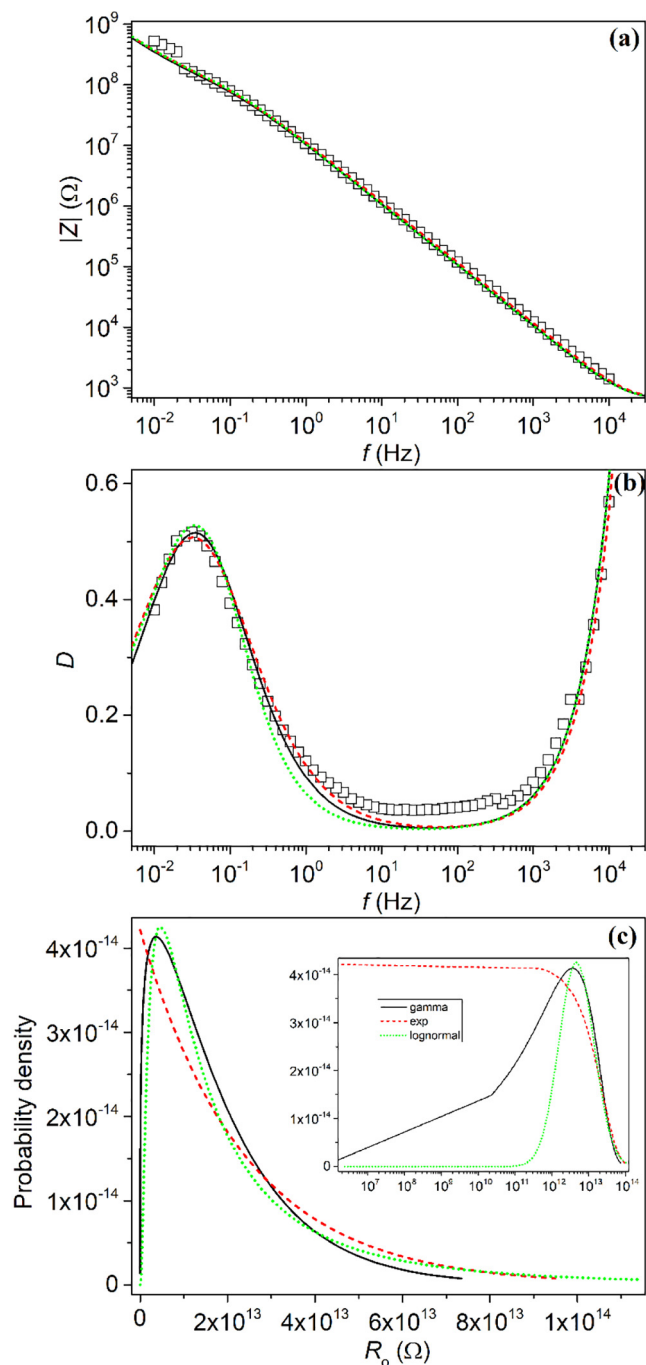


**Fig. 9.** Experimental (symbols) and modeled (lines) results of the frequency-dependence of  $|Z|$  (a) and  $D$  (b). The measured EWD device is filled with the original purple oil. Three different distributions, the Gamma (black solid), the Exponential (red dash) and the Log-Normal (green dot) distributions of  $R_o$  are incorporated in the modeling. (c): Plot of the PDFs of the distributions on a linear (log for the inset) scale on the horizontal axis. The value of  $\sigma_d$ ,  $\epsilon_{ro}$ ,  $\epsilon_{rd}$ ,  $t_d$  and  $R_{ESR}$  is the same as that listed in Table 1. The value of the other modeling parameters is listed in Table 3. (For interpretation of the references to color in this figure legend, the reader is referred to the web version of this article.)

distributions to make the simulation results match the measured one. The deduced values of  $\sigma_o$  are all on the order of  $10^{-12}$  S/m. The deduced oil-film thickness is the largest when using the Exponential distribution. As shown in Fig. 9(a) and (b), both of the two distributions can be used to simulate the measured result as well. Fig. 9(c) is the plot of the PDFs on the log scale on the horizontal axis. It can be seen that the probability density of the Exponential distribution is the largest

below  $\sim 10^{12}$   $\Omega$ , while the smallest for the Log-Normal distribution. Despite the distinct difference in the low  $R_o$  regime, all the three PDFs yield similar probability density above  $\sim 10^{12}$   $\Omega$ . Unfortunately we have not yet been able to find the root cause of variation in the oil conductivity. Since each choice of PDF gives similar fit quality we cannot choose with confidence which is the most appropriate PDF to pick. Speculation about the contamination mechanism suggests that use of the log-normal distribution is an acceptable choice.

The electrical conductivity of oil conductivity is very sensitive to impurities that can serve as charge carrier. What we concluded from our analysis is that geometric parameters such as variations in the oil film thickness is insufficient to explain the impedance data. Instead it is more likely that each pixel has a different level of impurity. Because the stock solution is mixed well we cannot expect that the already present charge carriers in the stock solution distribute themselves with different concentrations in the different pixels, what would be expected in that case is a Gaussian distribution with very narrow width. It is most likely that the source of variation fundamentally are defects during the process that are impacted by particles. A particle could perhaps influence the litho-process locally, and as a result unintendedly produced charge carriers will leach in the oil after filling. If this generation of charge carriers coupled with the presence of particles is indeed the root cause, one expects the particle size distribution of particulate contamination to underly the distribution of conductivities. Since quite often particulate contamination is found to be having a Log-Normal distribution of sizes [30], a Log-Normal distribution of the conductivities may also be expected. Note that the above is speculation, we have no proof of the above.

The effect of the standard deviation ( $\sigma$ ) of the Log-Normal distribution on the simulation result is also examined. Similar to the Gamma distribution, the larger  $\sigma$  is, the more broadened the Log-Normal PDF becomes, thereby leading to larger  $f_{peak}$ , smaller  $D_{peak}$  and larger  $W_{peak}$ . The rate parameter ( $\lambda$ ) of the Exponential distribution is the reciprocal value of the average  $R_o$  which is determined by  $\sigma_o$ . Hence, the shape of the Exponential distribution PDF cannot be varied independently. The same effect of  $\sigma_o$  on the simulation result is found for the Exponential and the Log-Normal distributions. Moreover, the dependence on  $\sigma_o$  of the peak position is consistent with the effect of the shape of the PDFs of the three distributions on the modeled result. When the PDFs of the Gamma or Log-Normal distributions become more broadened, or the rate parameter of the Exponential distribution increases, the number of the pixels with smaller  $R_o$  increases, which is therefore similar to directly decreasing  $\sigma_o$ , both causing the peak position shift to the right.

## Conclusion

An EWD device was fabricated and its frequency dependences of the impedance and the dissipation factor were measured. Modeling of the measurement result based on an equivalent circuit model was also performed. It is revealed that the position of the peak of the dissipation factor increases with the oil conductivity, which is also demonstrated in the measured results of the EWD devices with the high-conductivity-oil. It is found that the broadness of the measured dissipation peak cannot be reproduced in the modeled result by tweaking modeling parameters without adopting any distribution of the oil-film resistance. Therefore, a distribution of oil-film resistance was incorporated into the equivalent analog circuit of the EWD device in order to model the measured frequency dependence in actual EWD devices. Three different types of distributions, the Gamma, the Exponential and the Log-Normal distributions, were tested in the modeling with the result showing that all the distributions can simulate the measured result. When the probability density function is broadened, the peak in the dissipation factor becomes lowered and broadened. The peak position shifts to the higher-frequency regime because the oil-film resistance of most pixels is

decreased when the probability density function is broadened. From the impedance data alone, it cannot be concluded which type of distribution matches the real situation the best. Hence, it is necessary to investigate and find reasons that lead to variation in the oil-film resistance to fully understand the statistical distribution of the pixels and eliminate the non-uniformity of the oil conductivity of the EWD device as much as possible. The results demonstrated in this report also suggest that the oil conductivity and degree of the distribution of the oil-film resistance can be estimated by measuring the frequency-dependences of the impedance and the dissipation factor. This technique is beneficial to characterize the correlation between oil conductivity and device property. For example, the aging of EWD is closely related to the properties of dye molecules in the oil. Yet, so far, there is no reliable test method. Our work provides a new approach to study in situ the relationship between oil conductivity and the aging process changes EWD.

#### CRedit authorship contribution statement

**Bojian Xu:** Conceptualization, Methodology, Software, Methodology, Writing - original draft, Formal analysis. **Yuanyuan Guo:** Data curation, Validation, Investigation. **Jitesh Barman:** Writing - review & editing. **Ben H. Ern :** Validation. **Yong Deng:** Visualization. **Guofu Zhou:** Supervision. **Jan Groenewold:** Conceptualization, Writing - review & editing.

#### Declaration of Competing Interest

The authors declare that they have no known competing financial interests or personal relationships that could have appeared to influence the work reported in this paper.

#### Acknowledgments

This work was supported by National Key R&D Program of China (No.2016YFB0401502), Program for Chang Jiang Scholars and Innovative Research Teams in Universities (No. IRT\_17R40), Science and technology project of Guangdong Province (No. 2018A050501013), Science and Technology Project of Shenzhen Municipal Science and Technology Innovation Committee (GQYCZZ20150721150406), Longhua District Technological SMEs Technological Innovation Project (20171228A1300902), Guangdong Provincial Key Laboratory of Optical Information Materials and Technology (No. 2017B030301007), MOE International Laboratory for Optical Information Technologies and the 111 Project, Natural Science Foundation of Guangdong (2018A0303130059).

#### Appendix A. Supplementary data

Supplementary data to this article can be found online at <https://doi.org/10.1016/j.rinp.2020.103223>.

#### References

- [1] R. A. Hayes and B. J. Feenstra, *Nature* 425, 383 (2003).
- [2] Shui L, Hayes RA, Jin M, Zhang X, Bai P, Van Den Berg A, et al. *Lab Chip* 2014;14:2374.
- [3] Sureshkumar P, Bhattacharyya SS. *J Adhes Sci Technol* 2012;26:1947.
- [4] Lu Y, Sur A, Pascente C, Ravi Annapragada S, Ruchhoeft P, Liu D. *Int J Heat Mass Transf* 2017;106:920.
- [5] Roghair I, Musterd M, van den Ende D, Kleijn C, Kreutzer M, Mugele F. *Microfluid Nanofluidics* 2015;19:465.
- [6] Mugele F. *Soft Matter* 2009;5:3377.
- [7] Li X, Tian H, Shao J, Ding Y, Chen X, Wang L, et al. *Adv Funct Mater* 2016;26:2994.
- [8] Mugele F, Baret J-C. *J Phys Condens Matter* 2005;17:R705.
- [9] Guo Y, Deng Y, Xu B, Henzen A, Hayes R, Tang B, et al. *Langmuir* 2018;34:11943.
- [10] Zhao Q, Tang B, Dong B, Li H, Zhou R, Guo Y, et al. *J Phys D Appl Phys* 2018;51.
- [11] Giraldo A, Massard R, Mans J, Derckx E, Aubert J, Mennen J, et al. *Dig Tech Pap* 2011;42:114.
- [12] Kilaru MK, Heikenfeld J, Lin G, Mark JE. *Appl Phys Lett* 2007;90.
- [13] Klingner A, Buehrle J, Mugele F. *Langmuir* 2004;20:6770.
- [14] Chiu Y-H, Liang C-C, Chen Y-C, Lee W-Y, Chen H-Y, Wu S-H. *J Soc Inf Disp* 2011;19:741.
- [15] Liang C-C, Chen Y-C, Chiu Y-H, Chen H-Y, Cheng W-Y, Lee W-Y, et al. *Dig Tech Pap* 2010;40:375.
- [16] Luo ZJ, Zhang WN, Liu LW, Xie S, Zhou GF. *J Soc Inf Disp* 2016;24:345.
- [17] J. Feenstra, R. Van Dijk, and R. Hayes, *US Patent* 8,154,486 (2012).
- [18] Thomas D, Audry MC, Thibaut RM, Kleimann P, Chassagneux F, Maillard M, et al. *Thin Solid Films* 2015;590:224.
- [19] Chevalliot S, Heikenfeld J, Member S, Clapp L, Milarcik A, Vilner S. *J Disp Technol* 2011;7.
- [20] H. H. Girault, in *Mod. Asp. Electrochem.*, edited by J. O. Bockris, B. E. Conway, and R. E. White (Springer US, 2011), pp. 1–62.
- [21] Homolka D, Mareček V, Samec Z, Baše K, Wendt H. *J Electroanal Chem* 1984;163:159.
- [22] Prasad M. *Electrokinetics of Nonpolar dispersions for electrophoretic displays and liquid. Toner Print* 2017.
- [23] F. Beunis, F. Strubbe, O. Drobchak, T. Brans, and K. Neyts, in *10th Int. Symp. Electrokinet. Phenomena, Abstr.* (2012), p. 23.
- [24] Massard R, Mans J, Adityaputra A, Leguijt R, Staats C, Giraldo A. *J Inf Disp* 2013;14:1.
- [25] Hrubesh LW, Buckley SR. *MRS Proc* 1997;476:99.
- [26] Song CF, Wang Y, Wang S, Cui Z. *Int J Food Prop* 2016;19:2522.
- [27] Tanikella RV, Agraharam S, Bidstrup Allen SA, Hess DW, Kohl PA. *J Electron Mater* 2007;31:1096.
- [28] Banpurkar AG, Sawane Y, Wadhai SM, Murade CU, Siretanu I, van den Ende D, et al. *Faraday Discuss* 2017;199:29.
- [29] See Supplemental Material at [<https://doi.org/10.1016/j.rinp.2020.103223>] for the information of cumulative distribution of the measured oil-film resistance reported in Ref. [10], numerical integration method of incorporating a distribution in the oil-film resistance in the device modeling, complete equivalent circuit of the EWD device, effects of the dielectric constant of the oil-film and FP, the thicknesses of the oil-film and FP, the equivalent series resistance and the electrical conductivity of FP on the device modeling.
- [30] Kissa E. *Dispersions: characterization, testing, and measurement*. New York: Marcel Dekker Inc; 1999.